JACS
JOURNAL OF THE AMERICAN CHEMICAL SOCIETY
Article
pubs.acs.org/JACS

Accordion-like Oscillation of Contracted and Stretched Helices of Polyacetylenes Synchronized with the Restricted Rotation of Side Chains

Yoshiaki Yoshida,[†] Yasuteru Mawatari,[†,‡] Asahi Motoshige,[†] Ranko Motoshige,[†] Toshifumi Hiraoki,[§] Manfred Wagner,[∥] Klaus Müllen,[∥] and Masayoshi Tabata[†,‡,*]

[†]Department of Applied Chemistry, Graduate School of Engineering, Muroran Institute of Technology, 27-1 Mizumoto-cho, Muroran, Hokkaido 050-8585, Japan

[‡]Research Center for Environmentally Friendly Materials Engineering, Muroran Institute of Technology, 27-1 Mizumoto-cho, Muroran, Hokkaido 050-8585, Japan

[§]Department of Applied Physics, Graduate School of Engineering, Hokkaido University, Sapporo, Hokkaido 060-8628, Japan

[∥]Max Planck Institute for Polymer Research, Ackermannweg 10, D-55128 Mainz, Germany

Supporting Information

ABSTRACT: A chiral substituted acetylene, (*s*)-2-octyl propiolate, was stereoregularly polymerized using a catalyst, $[Rh(nbd)Cl]_2$, at 40 °C in methanol to give the corresponding helical polymer, P*s*2OcP. The changes of ^1H and ^{13}C NMR spectra in line shapes and splitting patterns were consistently interpreted in terms of restricted rotation around the ester O−*C bond, ∼O−*C^{e}H^{e}(R)∼, R = a branched CH$^{e}_3$ in the ester side chains rather than the helix inversion with the aid of a 3-site jump model. Three peaks due to the branched methyl H^{e} proton and its C$^{\eta}$ carbon observed at 0 °C suggested the formation of three rotamers called A, B, and C, based on the presence of the contracted helix and stretched helix forms that have an intrinsic helical pitch. Furthermore, an accordion-like helix oscillation (HELIOS) along the main chain axis was proposed to explain the temperature dependence spectral changes observed in ^1H and ^{13}C NMR, UV−vis, and circular dicromism (CD) spectra. The temperature dependence UV−vis and CD spectra of P*s*2OcP corroborate the presence of contracted and stretched one-handed helix sense polymers in solution in which the helical pitches and their persistence lengths depend on the temperature.

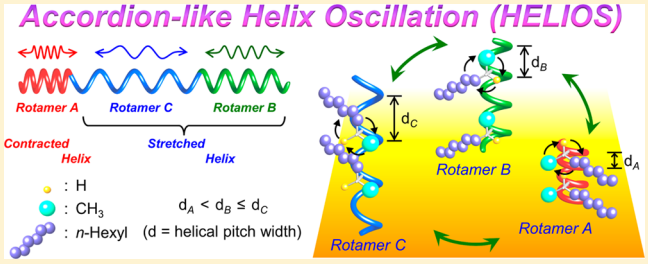

INTRODUCTION

During the past two decades, a few rhodium complexes, e.g., $[Rh(nbd)Cl]_2$-cocatalysts (nbd: norbornadiene), also called bidentate Rh catalysts,[1] including zwitterionic Rh complexes[2] and cationic $Rh^+BF_3^-$ complexes,[3] have been developed as important stereoregular polymerization catalysts for various substituted acetylene (SA) monomers to obtain helical substituted polyacetylenes (SPAs) with *cis*−*transoid* geometrical structures. Furthermore, it has been observed that a monodentate Rh complex (Rh catalyst) is generated in situ from the corresponding bidentate Rh complex when triethylamine, alcohol, or aqueous alcohol are used as either the cocatalyst, or the polymerization solvent which generates the propagation species of the Rh catalyst.[1,4] SPAs with helical *cis*−*transoid* main-chain structures are associated with chirotropic properties[5,6] and form pseudohexagonal crystals, called columnars,[1,4] which are driven by van der Waals forces in the solid state. Previously, poly(alkyl propiolate)s (PAPs) were reported to be promising oxygen-permeable materials[7] with neither siloxyl nor trialkylsilyl groups.[8,9] The helical pitch of an alkoxy substituted poly(phenylacetylene) can be controlled using external stimuli, e.g., thermal treatment or exposure to solvent vapor in the solid phase where the *cis*−*transoid* as a stretched helix rearranged to *cis*−*cisoid* as a contracted helix accompanied with a drastic change in color from blight yellow to dark red.[10] Thus, the detailed geometrical and spatial helical structures of SPA polymers should be explicitly and unequivocally determined to identify their functional properties such as their oxygen permeability,[7] nonlinear optical behavior,[11] electrical conductivity,[12] memory effects of spin glass materials,[13] and responsiveness to external stimuli.[14] Many helical polymers, including SPAs and polypeptides, have been used for effective separation of enantiomers.[15] Recently, the helix inversion of various SPAs with chiral side chains has been proposed based on CD spectral data.[5,6] In this report, we demonstrate a restricted rotation about an ester O−*C bond in the chiral side chain of helical poly((*s*)-2-octyl propiolate)

Received: January 16, 2013
Published: February 12, 2013

   dx.doi.org/10.1021/ja4004987 | *J. Am. Chem. Soc.* 2013, 135, 4110−4116

(Ps2OcP). We also propose that a 3-site jump rotation about the ester bond produces contracted and stretched helices accompanied by an *Accordion-like Helix Oscillation (HELIOS)*. The conformational structures corresponding to the 3-site jump were determined together with their helical pitches by using solution dynamic ^{1}H and ^{13}C NMR, infrared (IR), absorption (UV–vis), and circular dichromism (CD) techniques.

EXPERIMENTAL SECTION

Measurements. Number-average and weight-average molecular weights (M_n and M_w, respectively) of Ps2OcP polymers were measured using a JASCO GPC 900–1 equipped with two Shodex K-806L columns and an RI detector. Chloroform was used as an eluent at 40 °C, and poly(styrene) standards (M_n = 800–1 090 000) were employed for calibration. ^{1}H NMR (500 MHz) and ^{13}C NMR (125 MHz) spectra were recorded on a JEOL JNM-ECA500 using chloroform-d_1 ($CDCl_3$) and methylene dichloride-d_2 (CD_2Cl_2) as solvents at various temperatures. Tetramethyl silane (TMS) (Aldrich) was used as standard. Solution UV–vis and IR spectra of polymers were recorded on JASCO V570 and FT/IR 230 spectrophotometers, respectively, in methylene dichloride (CH_2Cl_2) at various temperatures. Solution CD spectra of polymers were taken on a JASCO J-720WI spectrometer in CH_2Cl_2 at various temperatures. Energetically optimized dynamic conformations of Ps2OcP were deduced from molecular mechanics calculations using the MMFF94 force field program (Wavefunction, Inc., Spartan '10 Windows version 1.1.0).[16] Spectral simulation of ^{1}H and ^{13}C NMR spectra and calculation of the restricted rates of rotation about the ester O–*C bond were performed using the gNMR program.[17]

Materials. Synthesis of (*s*)-2-octyl propiolate(***s*2OcP**) **1**. A mixture of 100 mL of toluene, 19.5 g (0.15 mol) of (*s*)-2-octanol (Tokyo Chem. Ind.), 7.0 g (0.10 mol) of propiolic acid (Aldrich), and 1.9 g (10.0 mmol) of *p*-toluenesulfonic acid (Tokyo Chem. Ind.) was refluxed for 8 h in a Dean–Stark apparatus. The resulting mixture was washed with saturated sodium hydrogen carbonate aqueous solution and distillated water. The organic layer was dried over anhydrous sodium sulfate and the solvent was removed by evaporation. The crude product was purified by distillation (90 °C/7 mmHg) to obtain a colorless liquid **1**, 12.2 g in 67% yield. ^{1}H NMR ($CDCl_3$): δ 5.01 (sext, J = 6.3 Hz, 1H, $OCH(CH_3)CH_2$), 2.85 (s, 1H, HC≡C), 1.72–1.46 (m, 2H, $OCH(CH_3)CH_2$), 1.36–1.31 (m, 6H, $(CH_2)_3$), 1.27 (d, J = 6.3 Hz, 3H, $OCH(CH_3)$), 0.88 (t, J = 6.3 Hz, 3H, CH_3); ^{13}C NMR (ppm): δ 152.9, 74.8, 74.6, 66.5, 31.7, 28.9, 28.4, 25.8, 22.6, 14.1.

Polymerization. Poly((*s*)-2-octyl propiolate), Ps2OcP, was obtained upon polymerization of (*s*)-2-octyl propiolate monomer (*s*2OcP) **1** using the catalyst, $[Rh(nbd)Cl]_2$, as shown in Scheme 1. In a typical procedure, 1.0 g (5.5 mmol) of the monomer and a calculated amount, 25 mg (5.5×10^{-2} mmol), of the catalyst were dissolved in MeOH (2.8 mL). The mixture was added to a specially designed U-shaped ampule[1a] and was stirred for 4 h at 40 °C. The resulting reaction mixture was poured into excess methanol with stirring. The resulting pale yellow polymer was washed with methanol and dried under dynamic vacuum, approximately 10^{-2} Torr, for 12 h at room temperature.

Scheme 1. Preparation of Ps2OcP with Rh Complex Catalyst

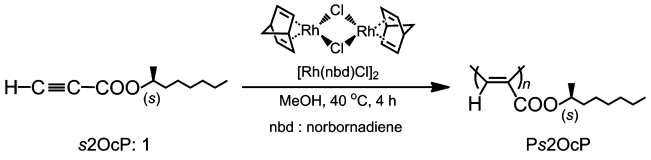

Poly((s)-2-octyl propiolate). ^{1}H NMR ($CDCl_3$): δ 7.15 (br., 1H, *H*C≡C), 4.78 (br., 1H, OC*H*), 1.63, 1.47 (br. d, 2H, $CH(CH_3)CH_2$), 1.29 (br., 8H, $(CH_2)_4$), 1.20 (br., 3H, $CH(CH_3)$), 0.88 (br., 3H, CH_3); ^{13}C NMR (ppm): δ 165.2, 139.1, 131.4, 72.6, 36.3, 32.3, 29.8, 25.9, 23.1, 19.8, 14.3. Anal. Calcd. for $C_{11}H_{18}O_2$: C, 72.49; H, 9.95. Found: C, 72.17; H, 9.95 (see Figure S1 of the Supporting Information, SI).

RESULTS AND DISCUSSION

Polymerization. The polymerization of **1** was performed using the catalyst, $[Rh(nbd)Cl]_2$, at 40 °C for 4 h in MeOH to obtain the corresponding polymer, Ps2OcP, as shown in Scheme 1 and Table 1. The polymer was produced in a moderate yield of 33%, a number-average molecular weight (M_n) of 5.7×10^4, a molecular weight dispersity (M_w/M_n) of 3.9, and the ratio of helical *cis–transoid* structure of 79%.[1,4]

Table 1. Synthesis of Poly((*s*)-2-octyl propiolate)s by a Catalyst $[Rh(nbd)Cl]_2$ in MeOH[a]

polymer	yield[b] (%)	M_n[c] (x10^{-4})	M_w/M_n[c]	*cis*[d] (%)
Ps2OcP	33	5.7	3.9	79

[a] $[M]_0$ = 2.0 mol/L, $[M]_0/[cat.]$ = 100. [b] Insoluble fraction in methanol. [c] Estimated by GPC analysis (PSt, $CHCl_3$). [d] Determined by ^{1}H NMR analysis (CD_2Cl_2).

Conformational Rotamers A, B, and C Detected by ^{1}H NMR. The proton signals at 7.15, 4.78, 1.63–1.47, 1.29, 1.20, and 0.88 ppm were assigned to H^{α}–C≡C, O*CH^{ε}, CH^{ζ}_2, $(CH_2)_4$, $OCH(CH^{\eta}_3)$, and CH_3, respectively (Figure 1a). Figure 1b shows the temperature-dependence ^{1}H NMR spectra

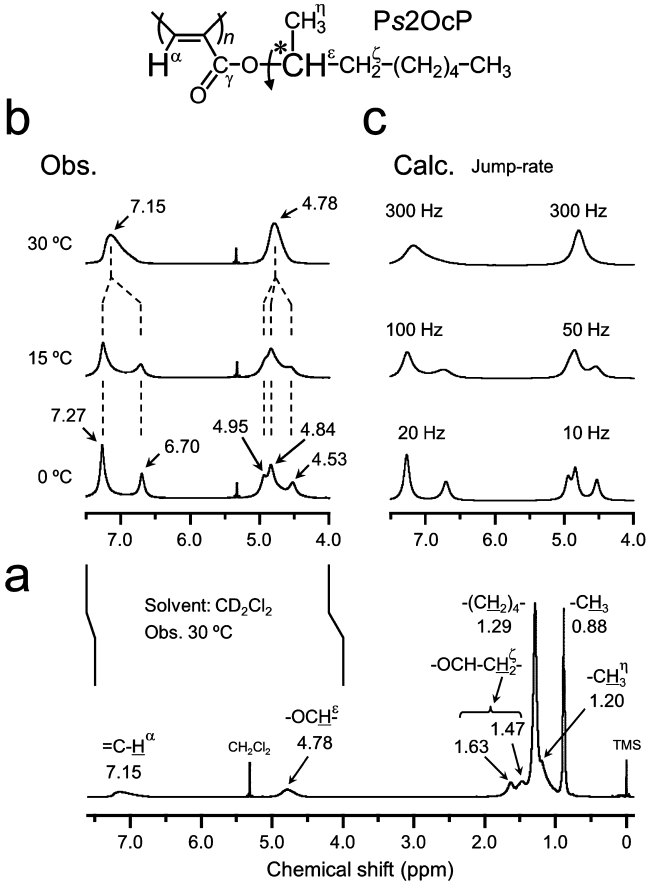

Figure 1. ^{1}H NMR spectra of Ps2OcP prepared with a catalyst, $[Rh(nbd)Cl]_2$, in MeOH at 40 °C. (a) observed at 30 °C, (b) expanded temperature-dependence spectra in the range of 7.5–4.0 ppm, and (c) computer-simulated spectra in the range of 7.5–4.0 ppm using a gNMR program.

dx.doi.org/10.1021/ja4004987 | J. Am. Chem. Soc. 2013, 135, 4110–4116

expanded in the range of 7.5−4.0 ppm. A fairly broad and distorted peak due to the methine H^{ε} roton was observed at 4.78 ppm at 30 °C, and the line shape of the peak gradually changed to give a triple line peak at 4.95, 4.84, and 4.53 ppm with a relative intensity of approximately 1:1:1 at 0 °C. Most notably, the line width of the H^{ε} signal decreased with decreasing temperature. The narrowing of the line width can be explained by the chemical site exchange phenomenon within P*s*2OcP and not by the helix inversion of the helical main chain of P*s*2OcP.[5] Hence, the restricted rotation about the ester O−*C bond through the 3-site jump in the side chain of P*s*2OcP occurs on the ^{1}H NMR time scale. Each conformer corresponding to the chemical site exchange is depicted using a Newman-like model, and referred to as rotamers A, B, and C, as seen in Figure 2. Therefore, the intensity of the triple line peak

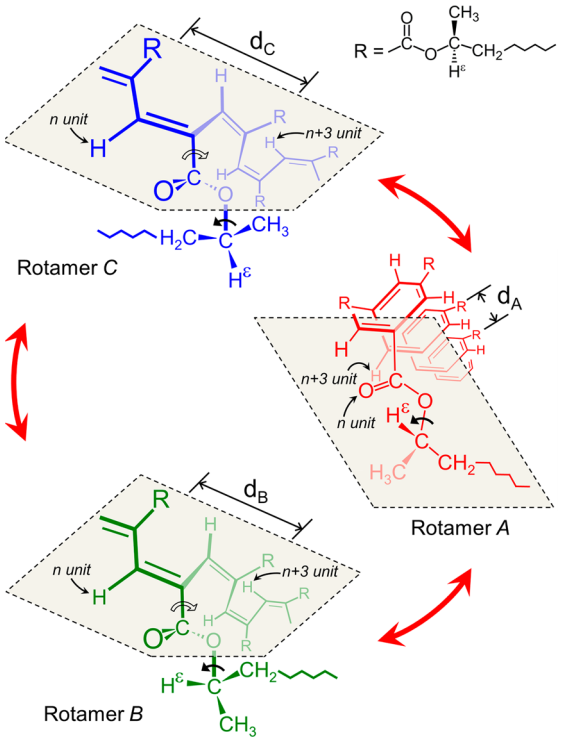

Figure 2. Perspective views showing helical structures including the vinyl proton and carbonyl moiety of rotamers A, B, and C.

observed at 0 °C indicates that rotamers A, B, and C are generated in an approximately equal amount. Conversely, the vinyl proton due to H^{α}−C═ was also separately observed as two peaks (7.27 and 6.70 ppm, relative intensity of approximately 2:1 at 0 °C) reflecting the different dihedral angle between the C═O and ═C−H^{α} bonds.[18,19] If rotamer A has an anti conformation between the main chain and the *n*-hexyl moiety in order to decrease steric hindrance, then a relatively narrow helix called a contracted helix is generated. Alternatively, rotamers B and C do not adopt these conformations due to steric reasons, and their pitch widths are expanded. From the chemical shifts of the two rotamers, it can be deduced that the rotamer absorbing at 6.70 ppm does not have the same pitch width as the rotamer absorbing at 7.27 ppm. The signal at 6.70 ppm is attributed to the contracted helices of rotamer A, and the one at 7.27 ppm to the stretched helices present in rotamers B and/or C. The latter have wider helical pitches than rotamer A. If rotamer A has a contracted helix, then the vinyl proton of rotamer A is located above the plane of the carbonyl C═O π bond at every *n*+3 monomer unit of the main-chain. Thereby, the narrow helical pitch causes a shielding of the vinyl proton (see Figure 2) as compared to rotamers B and C. Therefore, the ratio of the contracted helix, A, and the stretched helices, B and/or C, as formed in solution, can be estimated from Figure 1b as 1:2. The restricted ester O−*C rotation is also confirmed from the fact that no changes in chemical shifts and line widths of the remaining methyl branched hexyl side chain moieties occur, even when the temperature is increased from 0 to 30 °C (see Figure S2 of the SI).

The restricted ester O−*C bond rotation can be explained by the increasing double bond order of the ester O−*C single bond as a result of the extended conjugation. The observed three line peaks coalesce at 30 °C in CD_2Cl_2, in which a relatively fast ester O−*C bond rotation occurs, as shown in Figures 1b and 2. To the best of our knowledge, this is the first reported case of such a restricted ester O−*C bond rotation in synthetic polymers, although restricted rotation is well-known in the case of low-molecular amides.[18,19]

Rate of Restricted Rotation and Energy Barrier about the O−*C Bond. ^{1}H NMR spectral simulations were performed with the gNMR program[17] to determine the energy barrier of rotation around the ester O−*C bond, Gibbs' free energy, $\Delta G^{\ddagger}$, together with the rotational jump rate, τ, assuming a 3-site jump model,[18] i. e., the equal jump rate and equal population. The observed spectra reasonably agree with the simulated spectra at each temperature with respect to line shape and intensity (Figure 1c). The peak separation due to the vinyl proton was experimentally estimated to be 283 Hz at 0 °C (Figure 1b). The exchange jump rate between the peaks at 7.27 ppm and 6.70 ppm was determined as 20 Hz, which is associated with a free energy of the rotation of $\Delta G^{\ddagger}$ = 13.9 kJ/mol.

Rotamers A, B, and C Detected by ^{13}C NMR. The signals at 165.2, 139.1, 131.4, 72.6, and 19.8 ppm as well as the other 6 peaks at higher field in the ^{13}C NMR spectrum of P*s*2OcP at 30 °C (Figure 3a) were ascribed to a carbonyl carbon, γ; two vinyl carbonyl carbons, α and β; a methine carbon, ε; a branched methyl carbon, η; and six *n*-alkyl chain carbons (see Figure S3 of the SI), respectively. The temperature-dependent spectra expanded in the ranges of 170−125 ppm and 22−18 ppm are shown in Figure 3b. It appears that the degree of steric hindrance in the proposed rotamers A, B, and C takes the following order (see Figures 2).

$$A < B \leq C \quad (1)$$

In rotamers B and C, the *n*-hexyl chains stay more or less on the same side as the polymer main chain, which produces a relatively large steric hindrance, even though the chain direction is opposite. In rotamer A, the hexyl chain and the main chain adopt the *anti-zigzag* conformation. As a consequence, the dihedral angle between the main chain C═C bond and the ester moiety, ∼O−C═O∼, becomes small compared to that of rotamers B and C because of the narrow helical pitch. The alkyl side chain including the methyl group increases the electron density on the carbonyl carbon, although the C═C bond decreases the electron density on the ester carbon to some extent. Therefore, the peak observed at 166.6 ppm is assigned to the contracted helix of rotamer A. Alternatively, the helical pitch of rotamers B and C is wider than that of rotamer A, and thus, the dihedral angle between the C═C bond and the ∼O−

dx.doi.org/10.1021/ja4004987 | J. Am. Chem. Soc. 2013, 135, 4110−4116

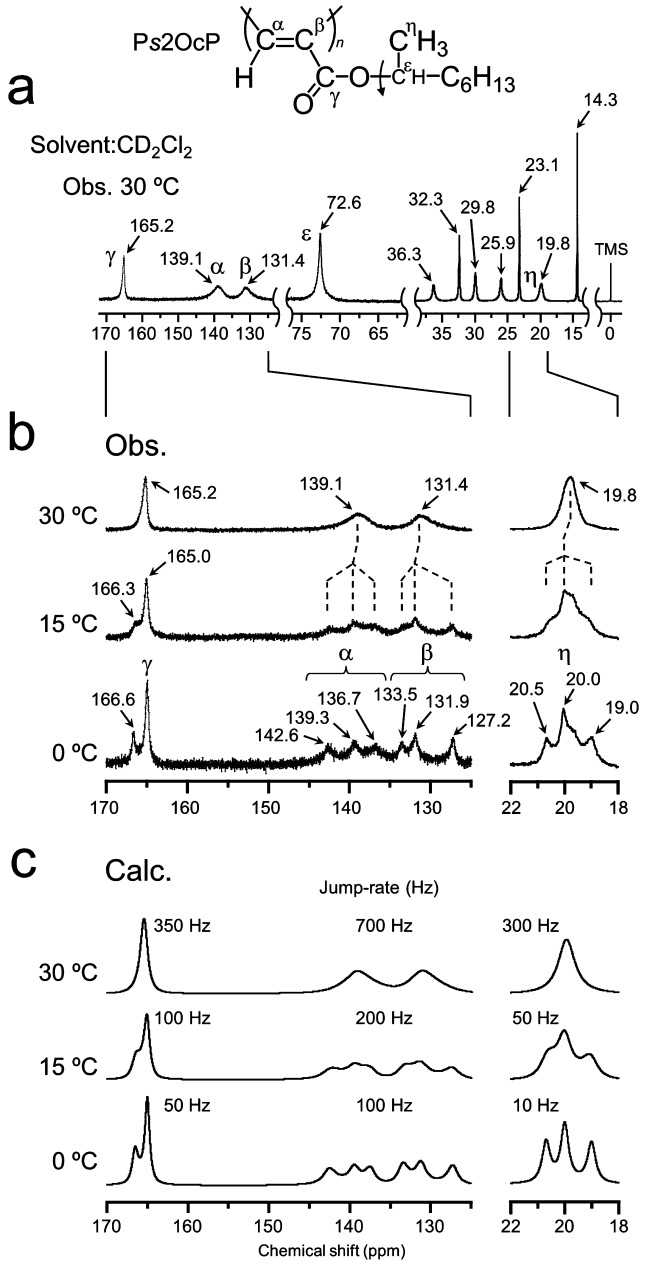

Figure 3. ^{13}C NMR spectra of Ps2OcP. (a) observed at 30 °C, (b) expanded temperature-dependence spectra in the ranges of 170−125 and 22−18 ppm, and (c) computer-simulated spectra using a gNMR program.

C═O∼ moiety is fairly large compared to that of rotamer A. In other words, the ester moiety is out of plane with the C═C bond plane. In rotamer B, the carbonyl carbon and the methyl moiety adopt a *trans zigzag* conformation, and the electron density on the carbonyl carbon is increased because of an I effect due to the methyl moiety. In rotamer C, the electron density on the carbonyl carbon remains unaffected because the methyl and the *n*-hexyl moieties do not possess an anti conformation (Figure 2).

Therefore, the peak observed at 165.0 ppm was attributed to rotamers B and/or C as the stretched helices. Thus, the C^{γ}═O carbon signal was observed at 166.6 and 165.0 ppm, and the approximate intensity ratio of 1:2 can reasonably be explained. This finding indicates that three types of helices have been generated: one contracted helix and two stretched helices. Two broad signals due to the α and β carbons in the main-chain C═C bond at 30 °C were also split at 0 °C into three peaks: namely 142.6, 139.3, and 136.7 for the α carbon and 133.5, 131.9, and 127.2 ppm for the β carbon. Rotamer A has a *trans zigzag* plane, including a C^{α}═C^{β}−C^{γ}−O−*$C^{\varepsilon}R^1$ (R^1 = *n*-hexyl) bond that increases the electron density of both the α and β carbons. Therefore, the vinyl carbons observed at 136.7 and 127.2 ppm were attributed to rotamer A. Rotamer C does not adopt such a trans zigzag conformation between the methyl carbon C^{η} and *n*-hexyl carbon chain moiety, and therefore, the peaks at 142.6 and 133.5 ppm were attributed to rotamer C (Figures 2 and 3b). The peaks at 139.6 and 131.9 ppm were assigned to rotamer *B*. The simulated temperature-dependent ^{13}C NMR spectra agreed well with the observed spectra (see Figure 3c). The rotational jump rate, τ, at each carbon is shown in Figure 3c. Three peaks due to the branched methyl carbon, C^{η}, were also observed at 0 °C, and only a broad singlet peak was observed at 30 °C. These signal changes were also interpreted in terms of the generation of the rotamers A, B, and C. In rotamer B, the carbonyl carbon, C^{γ}, and methyl carbon, C^{η}, in the −O−C^{ε}−$C^{\eta}H_3$ moiety exist in a *trans zigzag* structure; thus, the methyl carbon C^{η} peak should be observed at a lower magnetic field, 20.5 ppm. In contrast, the peak at 19.0 ppm was attributed to rotamer C because no such *zigzag* conformation was observed. Therefore, the peak 20.0 ppm, was attributed to rotamer A.

The negative charges on each carbon calculated by the Hartree−Fock 3-21G method were determined to be rotamer *B* = 0.574, rotamer *A* = 0.602, and rotamer *C*═0.617, respectively,[24] whose charge order agreed with the observed chemical shift of their carbonyl groups. Thus, it clearly follows from the temperature-dependent ^{1}H and ^{13}C NMR spectra that rotamers *A*, *B*, and *C*, which have an intrinsic pitch width and helical main chain length, or persistence length, are undoubtedly generated with a dynamically and spatially favorable conformational structure on the prevailing time scales. Every pitch length of the helical rotamers is dynamically oscillating, or synchronized, with the rotation around the ester O−*C bond. Therefore, we propose that this phenomenon is called an *Accordion-like Helix Oscillation (HELIOS)* of the PAP Main Chains. Conformational and spatial information regarding the ester carbonyl moiety of each rotamer was also obtained from the IR spectra (Figure 4). Only one strong and broad peak was observed at 1714 cm^{-1}, which is an average value of

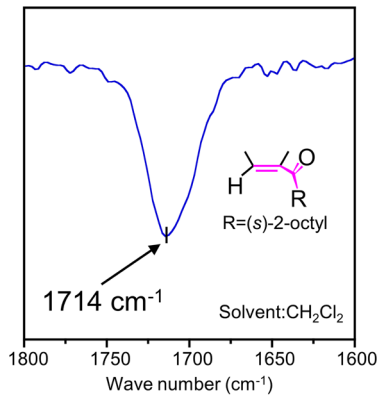

Figure 4. IR spectrum of the carbonyl group of Ps2OcP observed in CH_2Cl_2 at room temperature.

dx.doi.org/10.1021/ja4004987 | J. Am. Chem. Soc. 2013, 135, 4110−4116

the *cis* and *trans* vinyl carbonyl absorptions (e.g., 1729 and 1704 cm^{-1} of the model compounds)[20,21] (see Figure S4 of the SI). The presence of a broad peak suggests conformational exchanges of the carbonyl carbon among rotamers A, B, and C, as mentioned above.

UV and CD spectra of Contracted and Stretched Helices. Two absorption maxima, λ_{max}, were observed at 30 °C (Figure 5). The absorption at 371 nm was red-shifted, i.e., it

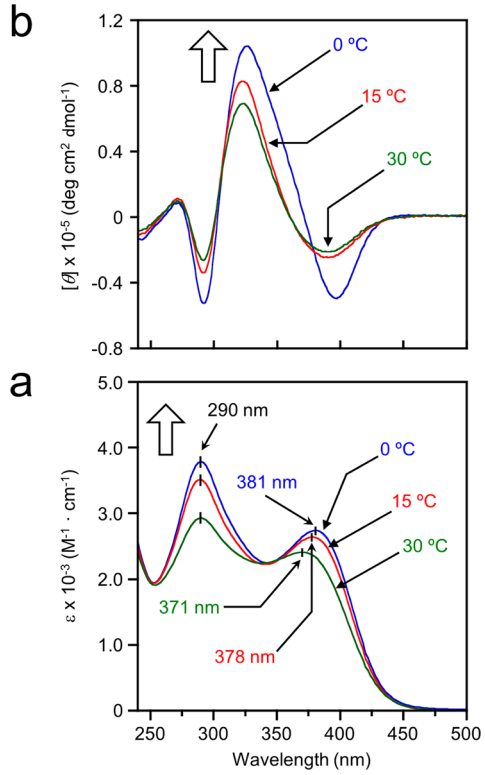

Figure 5. Temperature-dependence UV−vis and CD spectra of P*s*2OcP. (a) UV−vis spectra in CH_2Cl_2 and (b) CD spectra of P*s*2OcP observed in CH_2Cl_2.

was at 381 nm when observed at 0 °C, and the absorption intensity increased from 30 to 0 °C. The absorption intensity at 290 nm was greatly enhanced, keeping the absorption position at 0 °C. If the pitch width of the stretched helix within a limited main-chain length is thermally and reversibly oscillating, then its average pitch width becomes smaller because the degree of the stretched helix component is decreased. Therefore, it can be deduced that the effective conjugation length due to the stretched helix in the main chain of P*s*2OcP is decreased. This decrease is the reason why λ_{max} at 381 nm is blue-shifted, decreasing the absorption intensity when heated. It is assumed that the λ_{max} of a rotamer having a wider helical pitch is red-shifted compared with a rotamer with a narrow helical pitch.[22] On the contrary, the pitch width of the contracted helix also thermally oscillates, then its average pitch width become wider because the degree of the contracted helix, i.e., helicity is decreased, although the oscillation degree of the contracted helix is relatively small and limited compared with those of the stretched helices. Therefore, it is easily deduced that the helicity, i.e., the absorption intensity due to the contracted helix is decreased when observed at 30 °C as seen in Figure 5a. This also indicates that the resulting contracted helix has a narrow coherent and limited pitch width unlike that of the stretched helix pitch width as discussed below. Thus, this limitation is the reason why the absorption position at 290 nm is kept even when observed at 0 °C as shown in Figure 5a. Therefore, the absorption at 290 nm can be reasonably assigned to that of the contracted helix, although the correct absorption coefficients of each helix are not known.

Thus, two absorptions at 290 and 371 nm were reasonably attributed to the contracted helix, rotamer A, and stretched helices, rotamers B and/or C, of P*s*2OcP, respectively. Further, the temperature-dependent UV−vis spectral changes could be explained by assuming that the helical chain rapidly oscillated, exchanging the helical pitch width between the contracted and stretched sequences within a limited helical main chain length (see Figure 6). Previously, the λ_{max} observed at a shorter

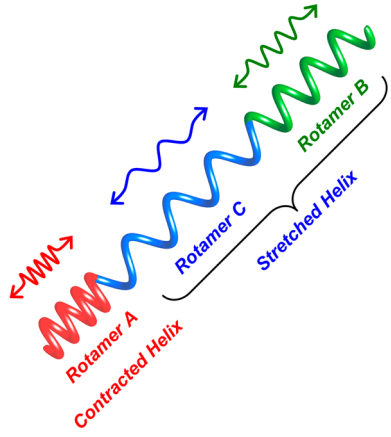

Figure 6. Proposed image model for the contracted helix and stretched helix main chain.

wavelength was attributed to the random coil of a one-handed helix sense polymer,[23] where an inversion of the helix sense of the main chain was assumed. However, it seems that ^1H or ^{13}C NMR spectral data do not support the existence of such a random coil, even at 30 °C.[23]

CD spectra of P*s*2OcP were observed in order to determine the helicity and degree (Figure 5b). The CD spectra showed the Cotton effect at 325 nm whose intensity greatly increased at lower temperature. Therefore, the helicity of the main chain was increased at lower temperature, and the ratio of a one-handed helix with a more tightly wound main chain is increased. If helix inversion for P*s*2OcP occurred rapidly along the main chain helix, then inversion of the Cotton effect sign should be observed at 30 °C. At this temperature, the ester proton together with the vinyl proton of ^1H NMR coalesced to symmetrical and unsymmetrical broad peaks at 30 °C, respectively.[5] However, no such signal inversion was detected in the CD spectra,[22] even at 30 °C, as shown in Figure 5b. This result strongly indicates that rather a restricted ester O−*C bond rotation occurs. Thus, the temperature-dependence UV−vis and CD spectra allow us to conclude that the main chain of the one-handed helix sense polymer, P*s*2OcP, never undergoes helix inversion under these experimental conditions.

Calculated Pitch for Contracted and Stretched Helices. Dihedral angles between the two double bonds, the helical pitches, and the strain energies of P*s*2OcP were calculated using the MMFF94 force field program (Table 2).[16] The most stable rotamer among the three rotamers, A, B, and C was identified as A, assuming the 3-site jump model and an equal distribution ratio at each site. The calculation showed

dx.doi.org/10.1021/ja4004987 | *J. Am. Chem. Soc.* 2013, 135, 4110−4116

Table 2. Dihedral Angles between C−C and C═C Bonds, Helical Pitches, And Strain Energies of P*s*2OcP[a]

polymer	rotamer	dihedral angle (deg)	pitch (Å)	strain energy (kJ/mol·unit)
	A	70	3.6	230
P*s*2OcP	B	110	5.1	243
	C	140	5.3	311

[a]Calculated by Molecular Mechanics method (MMFF94).

that rotamer A determined as a contracted helix, has the smallest pitch width, 3.6 Å, and strain energies, 230 kJ/mol·units. Rotamers B and C are classified as stretched helices and have pitch widths of 5.1 Å and 5.3 Å and strain energies of 243 kJ/mol·units and 311 kJ/mol·units, respectively (see Figure 6 and Table 2).

Importance of PAPs with a Contracted Helical Pitch. SPAs, including P*s*2OcP, are classified as some of the stiffest helical polymers because they are composed of alternating C−C and C═C conjugated bonds and present additional π-conjugation due to π-stacking, which is generated in the direction of the molecular axis.[10] The calculated helical pitch width of the rotamers is approximately 3.6−5.3 Å (see Table 2), and the smallest pitch is comparable to the layer distance of graphites, 3.35 Å, which are electrically conductive materials.[25] In the case of poly(ethyl propiolate), the electrically current was measured to be approximately 10^{-8} A without doping.[26]

CONCLUSIONS

(*S*)-2-octyl propiolate, *s*2OcP (**1**), a chiral alkylpropiolate, was stereoregularly polymerized by using the catalyst $[Rh(nbd)Cl]_2$ at 40 °C in methanol to obtain the corresponding polymer, P*s*2OcP, which has a helical *cis*−*transoid* structure. The line shape and splitting pattern changes seen in the temperature-dependent ^1H and ^{13}C NMR indicated the presence of restricted rotation about the ester O−*C bond for ∼O−*C$^{\varepsilon}$H$^{\varepsilon}$(R)∼, R = CH$^{\varepsilon}_3$. It did however not support the helix inversion model.[5,22,23] The three peaks for the H$^{\varepsilon}$ proton and the C$^{\eta}$ carbon observed at 0 °C suggested the formation of three rotamers, A, B, and C, due to the presence of a contracted helix and two stretched helix forms. All of them possessed an intrinsic helical pitch, as confirmed by the MMFF94 and gNMR programs. Furthermore, an accordion-like helix oscillation (HELIOS) along the main-chain axis was proposed to explain the temperature-dependent changes observed in ^1H and ^{13}C NMRs, UV−vis, and CD spectra (Figure 7). The two UV absorption peaks also supported three such helices which were identified from temperature-dependent CD spectra as contracted and stretched one-handed helix sense polymers.[5,6,22] The smallest helical pitch width, 3.6 Å for P*s*2OcP, was close to that of graphite, a typical conductive and layered material. The present study will be very useful for the fabrication of a single helical molecule polymer device. We are currently studying the preparation of related helical polymers and their conventional spectroscopic features, such as electron spin resonance (ESR), to understand the contracted and stretched helix structures showing the HELIOS phenomena. The results will be published elsewhere soon.

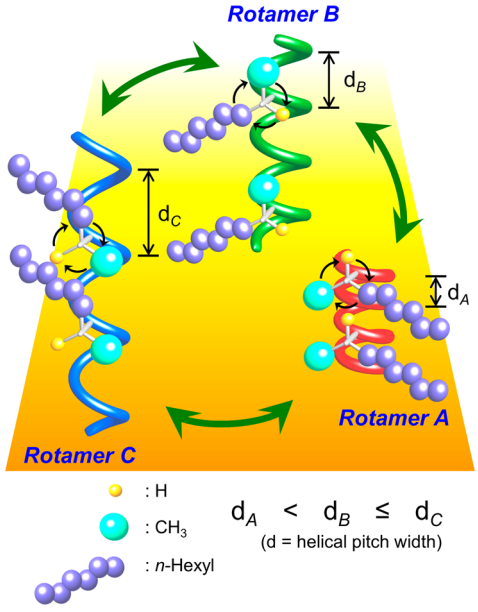

Figure 7. Stereo view for an accordion-like helix oscillation (HELIOS) between rotamers A, B, and C.

ASSOCIATED CONTENT

Supporting Information

Full scale spectral data of materials. This material is available free of charge via the Internet at http://pubs.acs.org.

AUTHOR INFORMATION

Corresponding Author

tabata@mmm.muroran-it.ac.jp

Notes

The authors declare no competing financial interest.

ACKNOWLEDGMENTS

We are grateful for the financial support of Dr. Y. Yoshida from the Muroran Institute of Technology. Thanks are extended to the Instrument Center at the Institute for Molecular Science for collecting the CD spectra measurements.

REFERENCES

(1) (a) Tabata, M.; Yang, W.; Yokota, K. *Polym. J.* **1990**, *22*, 1105−1107. (b) Yang, W.; Tabata, M.; Yokota, K. *Polym. J.* **1991**, *23*, 1135−1138. (c) Tabata, M.; Yang, W.; Yokota, K. *J. Polym. Sci., Part A: Polym. Chem.* **1994**, *32*, 1113−1120. (d) Lindgren, M.; Lee, H. S.; Yang, W.; Tabata, M.; Yokota, K. *Polymer* **1991**, *32*, 1532−1534.

(2) (a) Nomura, R.; Tabei, J.; Masuda, T. *J. Am. Chem. Soc.* **2001**, *123*, 8430−8431. (b) Gao, G. Z.; Sanda, F.; Masuda, T. *Macromolecules* **2003**, *36*, 3932−3937. (c) Zhang, W.; Tabei, J.; Shiotsuki, M.; Masuda, T. *Polym. Bull.* **2006**, *57*, 463−472. (d) Kishimoto, Y.; Itou, M.; Miyatake, T.; Ikariya, T.; Noyori, R. *Macromolecules* **1995**, *28*, 6662−6666. (e) Shiotsuki, M.; Sanda, F.; Masuda, T. *Polym. Chem.* **2011**, *2*, 1044−1058.

(3) Nakazato, A.; Saeed, I.; Katsumata, T.; Shiotsuki, M.; Masuda, T.; Zednik, J.; Vohlidal. *J. Polym. Sci., Part A: Polym. Chem.* **2005**, *43*, 4530−4536.

(4) (a) Tabata, M.; Kobayashi, S.; Sadahiro, Y.; Nozaki, Y.; Yokota, K.; Yang, W. *Macromol. Sci. Pure Appl. Chem.* **1997**, *A34* (4), 641−653. (b) Kozuka, M.; Sone, T.; Sadahiro, Y.; Tabata, M.; Enoto, T. *Macromol. Chem. Phys.* **2002**, *203*, 66−70.

(5) (a) Yashima, E.; Matsushima, T.; Okamoto, Y. *J. Am. Chem. Soc.* **1995**, *117*, 11596−11597. (b) Maeda, K.; Goto, H.; Yashima, E. *Macromolecules* **2001**, *34*, 1160−1164. (c) Nomura, R.; Fukushima, Y.; Nakako, H.; Masuda, T. *J. Am. Chem. Soc.* **2000**, *122*, 8830−8836. (d) Nomura, R.; Nakako, H.; Masuda, T. *J. Mol. Catal. A: Chem* **2002**, *190*, 197−205. (e) Yashima, E.; Maeda, K.; Iida, H.; Furusho, Y.; Nagai, K. *Chem. Rev.* **2009**, *109*, 6102−6211.

(6) (a) Tang, B. Z.; Kotera, N. *Macromolecules* **1989**, *22*, 4388−4390. (b) Sanda, F.; Masuda, T. *J. Syn. Org. Chem. Jpn.* **2008**, *66*, 757−764. (c) Shiotsuki, M.; Sanda, F.; Masuda, T. *Polym. Chem.* **2011**, *2*, 1044−1058. (d) Aoki, T.; Kaneko, T.; Teraguchi, M. *Polymer* **2006**, *47*, 4867−4892.
(7) Tabata, M.; Sadahiro, Y.; Inaba, Y.; Yokota, K. *Macromolecules* **1996**, *29*, 6673−6675.
(8) Masuda, T.; Higashimura, T. *Adv. Polym. Sci.* **1986**, *81*, 121−165.
(9) Masuda, T.; Isobe, E.; Higashimura, T.; Takada, K. *J. Am. Chem. Soc.* **1983**, *105*, 7473−7474.
(10) (a) Motoshige, A.; Mawatari, Y.; Yoshida, Y.; Seki, C.; Matsuyama, H.; Tabata, M. *J. Polym. Sci., Part A: Polym. Chem.* **2012**, *50*, 3008−3015. (b) Mawatari, Y.; Tabata, M. *J. Jpn. Soc. Colour Mater.* **2009**, *82*, 204−209. (c) Mawatari, Y.; Tabata, M.; Sone, T.; Ito, K.; Sadahiro, Y. *Macromolecules* **2001**, *34*, 3776−3782.
(11) (a) Neher, D.; Wolf, A.; Bubeck, C.; Wegner, G. *Chem. Phys. Lett.* **1989**, *163*, 116−122. (b) Bredas, J. L.; Adant, C.; Tacks, P.; Persoons, A.; Pierce, M. *Chem. Rev.* **1994**, *94*, 243−278. (c) Falconieri, M.; D'Amato, R.; Russo, M. V.; Furlani, A. *Nonlinear Opt.* **2001**, *27*, 439−442. (d) Tabata, M.; Sone, T.; Yokota, K.; Wada, T.; Sasabe, H. *Nonlinear Opt.* **1999**, *22*, 341−344. (e) Wada, T.; Wang, L.; Okawa, H.; Masuda, T.; Tabata, M.; Wan, M.; Kakimoto, M.; Imai, Y.; Sasabe, H. *Mol. Cryst. Liq. Cryst.* **1997**, *294*, 245−250.
(12) (a) Skotheim, T. A., Ed. *Handbook of Conducting Polymers*; Dekker: New York, 1986; Vols.*1*−*2*. (b) Ferraro, J. R.; Williams, J. M., Eds. *Introduction to Synthetic Electrical Conductors*; Academic Press Inc: New York, 1987. (c) Salomone, J. C., Ed. *Polymeric Materials*; CRC Press: New York, 1996; Vol. *8*.
(13) (a) Korshak, Y. V.; Medvedeva, T. V.; Ovchinnikov, A. A.; Spector, V. *Nature* **1987**, *326*, 370−372. (b) Tyutyulkov, N.; Müllen, K.; Baumgarten, M.; Ivanova, A.; Tadjer, A. *Synth. Met.* **2003**, *139*, 99−107. (c) Tabata, M.; Nozaki, Y.; Yang, W.; Yokota, K.; Tazuke, Y. *Proc. Jpn. Acad.* **1995**, *71*, 219−224. (d) Fisher, K. H.; Herz, J. A. *Spin Glass*; Cambridge University Press: Cambridge, 1991. (e) Pregjean, J. J.; Souletie, J. *J. Phys. (Paris)* **1980**, *41*, 1335−1352. (f) Floch, L.; Hammann, F.; Ocio, J.; Vincent, M. *Euro. Phys. Lett.* **1992**, *18*, 647−652. (g) Xenikos, D. G.; Multer, H.; Jouan, C.; Suilpice, A.; Tholence, J. L. *Solid State Commun.* **1997**, *102*, 681−685. (h) Tabata, M.; Watanabe, Y.; Muto, S. *Macromol. Chem. Phys.* **2004**, *205*, 1174−1178. (i) Watanabe, Y.; Muto, S.; Tabata, M. *Jpn. J. Appl. Phys. Part 2: Lett.* **2004**, *43*, 300−302.
(14) Maeda, K.; Yashima, E. *J. Syn. Org. Chem. Jpn.* **2002**, *60*, 878−890.
(15) (a) Nolte, R. J. M. *Chem. Soc. Rev.* **1994**, *23*, 11−19. (b) Cornelissen, J. J. L. M.; Rowan, A. E.; Nolte, R. J. M.; Sommerdijk, N. A. J. M. *Chem. Rev.* **2001**, *101*, 4039−4070. (c) Ito, Y.; Miyake, T.; Hatano, S.; Shima, R.; Ohara, T.; Suginome, M. *J. Am. Chem. Soc.* **1998**, *120*, 11880−11893. (d) Nakano, T.; Okamoto, Y. *Chem. Rev.* **2001**, *101*, 4013−4038. (e) Vogl, O. *CHEMTECH* **1986**, 698−703. (f) Ariga, K.; Kunitake, T. *Acc. Chem. Res.* **1998**, *31*, 371−378. (g) Abe, A.; Imada, Y.; Furuya, H. *Polymer* **2010**, *51*, 6234−6239.
(16) MMFF94 calculations were carried out with a Spartan'10 (Windows version 1.1.0), Wavefunction, Inc: CA.
(17) The simulations of NMR spectra were carried out with a gNMR program, ver. 5.0, Ivory Soft.
(18) (a) Fraenkel, G.; Franconi, C. *J. Am. Chem. Soc.* **1960**, *82*, 4478−4483. (b) Woodbrey, J. C.; Rogers, M. T. *J. Am. Chem. Soc.* **1962**, *84*, 13−16. (c) Gehring, D. G.; Mosher, W. A.; Reddy, G. S. *J. Org. Chem.* **1966**, *31*, 3436−3437.
(19) (a) LaPlanche, L. A.; Rogers, M. T. *J. Am. Chem. Soc.* **1963**, *85*, 3728−3730. (b) Neuman, R. C.; Roark, D. N.; Jonas, V. *J. Am. Chem. Soc.* **1967**, *89*, 3412−3416.
(20) Hesse, M.; Meier, H.; Zeeh, B. *Spectroscopic Methods in Organic Chemistry*; Linden, A., Martin, M., Eds.; Thieme Medical Pub.: Stuttgart, 2007.
(21) (a) Pretsch, E.; Bühlmann, P.; Affolter, C.; Shigeru, A. *Structure Determination of Organic Compounds*; Springer-Verlag: New York, 2004. (b) Silverstein, R. M.; Webster, F. X.; Kiemle, D. J. *Spectrometric Identification of Organic Compounds*, 7 th ed.; Araki, S., Mashiko, Y., Yamamoto, O., Kamada, T.; Wiley: New York, 2006.
(22) (a) Nomura, R.; Nakako, H.; Masuda, T. *J. Mol. Catal. A: Chem.* **2002**, *190*, 197−205. (b) Sanda, F.; Masuda, T. *J. Syn. Org. Chem. Jpn.* **2008**, *66*, 757−764. (c) Shiotsuki, M.; Sanda, F.; Masuda, T. *Polym. Chem.* **2011**, *2*, 1044−1058. (d) Yashima, E.; Maeda, K.; Iida, H.; Furusho, Y.; Nagai, K. *Chem. Rev.* **2009**, *109*, 6102−6211. (e) Aoki, T.; Kaneko, T.; Teraguchi, M. *Polymer* **2006**, *47*, 4867−4892.
(23) (a) Tabei, J.; Nomura, R.; Masuda, T. *Macromolecules* **2003**, *36*, 573−577. (b) Gao, G.; Sanda, F.; Masuda, T. *Macromolecules* **2003**, *36*, 3938−3943.
(24) Hartree-Fock(3-21G) calculations were carried out with a Spartan'10 Windows parallel ed., Wavefunction, Inc: CA.
(25) Spain, I. L. *The Physics of Semimetals and Narrow Band-Gap Semiconductors*; Carter, D. L., Bate, R. T., Eds.; Pergamon Press: Oxford, 1971.
(26) (a) Albrecht, O.; Sone, T.; Kuriyama, A.; Eguchi, K.; Yano, K. *Nanotechnology* **2008**, *19*, 505201. (b) Wang, N.; Zhang, Y.; Yano, K.; Durkan, C.; Plank, N.; Welland, M. E.; Unalan, H. E.; Mann, M.; Amaratunga, G. A. J.; Milne, W. I. *Nanotechnology* **2009**, *20*, 105201.